Stochastic Geometry Framework for Ultrareliable Cooperative Communications With Random Blockages

Gourab Ghatak, *Member, IEEE*, Saeed R. Khosravirad, *Member, IEEE*, and Antonio De Domenico

***Abstract*—We study an industry automation scenario where a central controller broadcasts critical messages to the wireless devices (e.g., sensors/actuators). We devise a stochastic geometry framework where the rate coverage probability of devices is modeled by taking into account the density of roaming blockages over the factory floor. To alleviate the loss in the coverage, we adopt a two-phase transmission policy, where in the *broadcast phase*, the central controller broadcasts the messages intended for the devices in the network area. The devices in coverage in the broadcast phase act as decode-and-forward relays in the *relay phase*, so as to reinforce the signal strength at the devices in outage. The total downlink transmission time is, therefore, partitioned into two phases by a tunable factor. Finally, we study the optimal value of the partitioning factor with varying device densities, blockage densities, and file sizes, and we highlight that a longer transmission time should be allotted to the broadcast phase in the case of larger file sizes or lower transmit power of the controller.**

***Index Terms*—Fifth generation (5G), Industrial Internet of Things (IIoT), stochastic geometry, ultrareliable low-latency communications (URLLC).**

I. Introduction

TRADITIONALLY, applications in an industrial setup, such as automated manufacturing, packaging, and on-field process monitoring, employ wired communications, e.g., Ethernet-based solutions [1]. These solutions can be expensive to deploy and cumbersome to maintain. Additionally, several of these applications require a highly flexible and dynamic communication infrastructure to support mobility [2], [3]. As a result, there is an increased interest to replace wired communication systems with wireless alternatives to reduce bulk as well as installation and maintenance costs [4].

The future industrial wireless networks will consist of a massive number of sensing, computing, and actuating devices that communicate with each other with ultrahigh reliability [5], [6]. Furthermore, for several applications such as critical control of these devices, the delay constraints on the control loop latency are of the order of a few milliseconds [7]. As a result, the communication link latency must be of the order of a millisecond, while, simultaneously, maintaining ultrahigh reliability. This comes under the purview of ultrareliable low-latency communications (URLLC) mode of operation in the fifth-generation (5G) ecosystem [8], [9]. The most important key performance indicators (KPIs) related to URLLC are latency, reliability, and availability. Traditional wireless networks are not optimized for such KPIs and thus, new enabling technologies, such as novel numerologies, flexible frame structure, link adaptation, and new diversity techniques, must be employed [5]. Additionally, with the advent of massive connectivity, ensuring reliability and latency for all the devices in the network is a challenge. In this regard, Shah *et al.* [10] have presented a protocol stack perspective for low latency and massive connectivity. As compared to wired connectivity, wireless solutions provide a possibility to incorporate a large number of nodes in the network while targeting the stringent URLLC KPIs.

On the downside, the presence of physical blockages or unfavorable channel conditions in the factory environment can severely degrade the received signal strength [11]. This may be detrimental, especially for URLLC applications. To address this issue, multihop transmission with cooperative relaying is proposed in [12], where devices with strong channel cooperate to provide a reliable communication link to devices in poor channel conditions. Here, we extend this work by assessing this protocol in a realistic industrial propagation environment, considering the effect of random blockages on the system performance. It must be noted that the deployment of dedicated relays can augment the performance of the devices in the networks. However, installation costs and the requirement of optimization of the number of locations of the dedicated relays with varying device densities make such a solution unattractive. On the contrary, our system benefits from devices already present in the network for relaying the signal. Specifically, as the network size grows, the number of potential relays also increases, which makes the solution scalable to any network size.

A. Related Work

Stochastic geometry has proven to be a key tool in the modeling and analysis performance metrics in large-scale

Manuscript received April 6, 2021; revised July 1, 2021 and August 3, 2021; accepted August 22, 2021. Date of publication August 30, 2021; date of current version March 24, 2022. *(Corresponding author: Gourab Ghatak.)*

Gourab Ghatak is with the Department of ECE, Indraprastha Institute of Information Technology Delhi, New Delhi 110020, India (e-mail: gourab.ghatak@iiitd.ac.in).

Saeed R. Khosravirad is with the Nokia Bell Labs, Murray Hill, NJ 07974 USA (e-mail: saeed.khosravirad@nokia-bell-labs.com).

Antonio De Domenico was with CEA-LETI, 38054 Grenoble, France. He is now with the Huawei Technologies, Paris Research Center, 92100 Boulogne-Billancourt, France (e-mail: antonio.de.domenico@huawei.com).

Digital Object Identifier 10.1109/JIOT.2021.3108955

2327-4662 © 2021 IEEE. Personal use is permitted, but republication/redistribution requires IEEE permission.
See https://www.ieee.org/publications/rights/index.html for more information.

Authorized licensed use limited to: CEA GRENOBLE. Downloaded on October 13,2022 at 10:28:49 UTC from IEEE Xplore. Restrictions apply.

networks. In the literature, stochastic geometry has been employed in the characterization of signal coverage, data rate, and localization performance of cellular [13] and *ad hoc* networks [14]. This follows from a statistical characterization of the signal-to-noise ratio (SNR) coverage probability of the users in the network by assuming appropriate spatial point process models for modeling the locations of network entities. In this work, we use tools from stochastic geometry to characterize the network reliability of the industrial automation system.

In order to enhance reliability, researchers have investigated time and frequency diversity, spatial diversity, and multidevice cooperation [12], [15], [16]. Li *et al.* [17] have studied adaptive transmission strategies to sustain services with different latency constraints. In particular, Swamy *et al.* [12] have shown that with multidevice cooperation, ultrahigh reliability can be achieved even in low or moderate signal-to-noise ratio (SNR) regime. Furthermore, they show that the target error rate, and consequently, the SNR necessary for achieving high reliability, cannot be achieved only by frequency diversity under realistic channel conditions. The protocol in [12] chooses a conservative transmission rate, set by the worst device's conditions. In this regard, Jurdi *et al.* [18] have proposed an adaptive rate selection scheme based on the instantaneous channel conditions. In their proposal, first, the channel states between the controller and the different nodes in the network are estimated. Then, the controller adapts the transmission rate for each node in the network to its instantaneous channel condition.

In [19], capacity and the coverage aspects of a factory automation setup are studied, by considering the effect of small- and large-scale fading. It is shown that equipping the devices with two antennas can dramatically reduce the required SNR for decoding and increase the capacity and the coverage of the network. The use of stochastic geometry to analyze URLLC system performance has been considered in the literature. Namely, the works in [20] analyze slicing of resources for URLLC and enhanced mobile broadband (eMBB) traffic transmission in a cellular network and [21] study different grant-free access solutions for URLLC.

To the best of our knowledge, the effect of roaming blockages in a wireless factory automation setup has not been investigated in the literature. In a typical factory environment, the presence of metal surfaces and high density of industrial machinery determines the multipath fading [22]. Moreover, static or moving devices can cause an obstruction and strongly attenuate signal strength [23]. In this article, we assess device cooperation for reliable industrial wireless control, taking into account the effect of channel blockages. We model the location of the devices and the blockages as random processes and use tools from stochastic geometry to analytically characterize the probability of a typical node to be under coverage with and without cooperation. Specifically, pertaining to the blockage process, Matérn [24] has studied two variants of repulsive point processes in his work. We use the Matérn hard-core process (MHCP) type II to model the locations of the centers of the blocking objects.

B. Contributions and Organization

The contributions of this article are as follows.

1) We characterize the blockage statistics of the communication links in an industrial wireless network by modeling the position of the blockages as points of an Matérn hard-core process (MHCP), which has not carried out in literature thus far. First, we use tools from stochastic geometry to characterize the SNR and the rate coverage probability of an arbitrarily located device in the network without multidevice cooperation. Remarkably, we show that even for sub-6-GHz transmissions, blockages play a key role in limiting the coverage, and hence, in network planning for industrial Internet of Things (IoT) networks.
2) We adopt the two-phase communication protocol to enable reliable industry automation services. Our results show that this policy significantly increases (by up to 25%) the coverage performance of the devices as compared to single transmission from the controller. In particular, we characterize analytically the rate coverage performance of a system using this cooperative protocol in an environment with random blockages.
3) We also study the trends of the optimal value of the resource partitioning factor with respect to the rate coverage probability with varying blockage densities, device densities, and file sizes. More specifically, we show that as the device density increases, more time should be allotted to the broadcast phase for maximizing the rate coverage if the data size depends on the number of devices. On the contrary, for a fixed data size broadcast, an increase in the number of devices necessitates an increase in the resources of the relay phase to limit the outage.

The proposed solution is applicable in the wide view to the trend of an industrial wireless control system design, where the traditionally wired communication between robots, machines, and controllers (e.g., fieldbus-based systems such as SERCOS, PROFIBUS, and WorldFIP) is expected to be replaced by wireless connections to enable seemless rearrangement of the factory floor depending on the production and manufacturing needs. Some examples can be seen in [25] and [26]. A recent example of industrial wireless control (in the era of industry 4.0 revolution) was announced in a joint effort between Nokia and Omron, where the former is planned to enable wireless connectivity solutions among mobile robots from Omron (see an online report in [27]).

The remainder of this article is organized as follows. In Section II, we introduce the system model, characterize the blockage process, and outline the transmission model. Then, in Section III, we derive the SNR and rate coverage probability of the test device. We present numerical results in Section IV on the performance of the network. Finally, this article concludes in Section V.

II. System Model

In this section, we describe the communications system, and we highlight the main assumptions we use in our analysis.

Authorized licensed use limited to: CEA GRENOBLE. Downloaded on October 13,2022 at 10:28:49 UTC from IEEE Xplore. Restrictions apply.

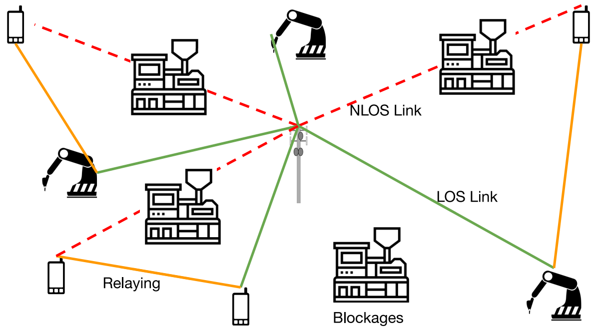

Fig. 1. Illustration of the considered system model. The green lines represent the LOS links, and the red dotted line represent the NLOS links. The orange line represents a relaying link.

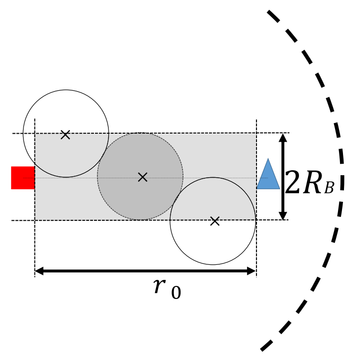

Fig. 2. Link-blockage illustration. The blue triangle is a device, and the red square is the controller. The dotted line is the cell boundary.

Network Model: We consider the factory area to be a closed bounded subset $\mathcal{S}$ of the 2-D Euclidean plane. For simplicity of the analysis, we assume $\mathcal{S}$ to be a disk[1] of radius R. As depicted in Fig. 1, we consider a multidevice wireless network where a controller located at the center of $\mathcal{S}$ broadcasts data to multiple devices distributed in the network area uniformly, with an intensity λ. Note that an additional challenge to modeling such finite domain networks is the absence of a *typical* device. Thus, we characterize the performance of a test device conditioned on its location in the network and then average out on all possible locations. We assume that the wireless links can be blocked by physical objects circularly shaped with a radius R_B (see Fig. 2), and whose locations are distributed in the network area according to an MHCP. This model, in contrast with the classic Poisson point process (PPP), ensures that there is a minimum distance between two nearby blockages, thereby enabling a more accurate model for physical objects. In the following, we carry out our analysis from the perspective of the test device in the network located at distance r_0 from the central controller.

Characterization of the Blockage Process: From the perspective of the test device, the link to the controller is blocked by a circular blockage of radius R_B, if at least one point of the circular blockage falls over the link connecting the test device and the controller. This is illustrated in Fig. 2, where a blockage occurs if the center of at least one circular blockage falls inside the shaded rectangular area (of size $r_0 \times 2R_B$). Furthermore, we consider the scenario with agile dynamic blockages. Consequently, during the transmission of the packets, a line of sight (LOS) link may observe different realizations of the blockage process.

Here, we give a brief overview of the derivation of the MHCP, and then we present the intensity of such a process. An MHCP is formed from a dependent thinning of a parent Poisson point process (PPP) ϕ_P of intensity λ_P [29]. First, each point $x_i \in \phi_P$ is marked independently with a random mark $\mathcal{M}_i \in (0, 1)$. Then, a point $x_i \in \phi_P$ is retained in the MHCP if and only if the ball of radius R_B and centered in x_i $B(x_i, R_B)$ does not contain any point of ϕ_P with marks smaller than $\mathcal{M}_i$. Mathematically, the MHCP is described as

$$\phi_B = \{x_i \in \phi_P : \mathcal{M}_i < \mathcal{M}_j \ \forall \ x_j \in \phi_P \cap B(x_i, R_B)\backslash x_i\}.$$

Lemma 1: The intensity of the blockage process is given by [29]

$$\lambda_B = \frac{1 - \exp\left(-\lambda_p \pi R_B^2\right)}{\pi R_B^2}. \tag{1}$$

Proof: See [29, eq. (5.57)]. ■

As depicted in Fig. 2, the link between the controller and a node located at a distance r from the controller is blocked if a point of ϕ_B falls in the shaded area. As the thinning of ϕ_P preserves the Poisson nature of ϕ_B, the probability that the center of at least one blocking object falls in the shaded area can be approximated using the void probability[2]

$$\mathcal{P}_B(r) \approx 1 - \exp(-2\lambda_B r R_B). \tag{2}$$

Transmission Policy: We deploy a two-hop transmission policy, inspired by [12], where the total transmission time T is divided into two time-orthogonal phases and the overall bandwidth W is used in both the phases. We assume that the connection set up between the controller and the devices is executed by the radio resource control (RRC) protocol at the network layer. The transmission policy described next is implemented in the MAC layer. Furthermore, we assume a synchronized system for the transmission between the controller and the devices in the network. Therefore, we consider that the two phases are split by a factor $0 \leq \beta \leq 1$, where phases I and II duration are βT and $(1-\beta)T$, respectively. Furthermore, we assume that the downlink messages intended for the factory devices are concatenated together into a message of size b bits. Depending of the type of data, b can have a fixed value or be a function of the number of devices in the network, i.e., $b = b_0 N_0$, where $N_0 = \lambda\pi R^2$ is the average number of devices in the network and b_0 denotes the message size in bits for each device.

In phase I, the controller broadcasts the concatenated message with rate $R_1 = [(b)/(\beta T)]$. Due to the presence of blockages and the impact of the path loss, the devices located

[1]We note that the theoretical analysis in this article can be further extended to the case of arbitrarily shaped polygon by using the methodology developed in [28].

[2]Note that this approximation employs the void probability of PPP and allows us to derive network dimensioning insights under the influence of blockages.

Authorized licensed use limited to: CEA GRENOBLE. Downloaded on October 13,2022 at 10:28:49 UTC from IEEE Xplore. Restrictions apply.

farther from the controller are expected to have a higher probability of outage during phase I. To improve the coverage performance, we assume that the devices under coverage in phase I act as decode-and-forward relays to forward the message to the rest of the devices in phase II. Let the point process representing the locations of the devices under coverage after phase I (or the relays) be denoted by Φ_1. In the second phase, a device in outage in phase I attempts to successfully decode the message leveraging the retransmission from one or multiple relays. The relays transmit the decoded message with a rate $R_2 = ([b]/[(1-\beta)T])$.

Relaying Model: After the broadcast phase, the system moves into the relay phase (phase II). Subsequently, we consider two schemes for phase II: 1) full coordination: each device under outage in phase I is assumed to receive the data from all the devices of ϕ_1 (i.e., the realization of Φ_1 in phase 1) along with the controller and 2) nearest-relay transmission: each device under outage in phase I receives the data from its closest device from ϕ_1. Incidentally, the closest relay is statistically also the best relay due to the smaller chance of having its link to the device blocked by a random blockage and for a smaller path loss impact from the shorter distance. It should be noted that, however, selecting the closest relay for each device in outage may be complex and require complex system coordination.

Propagation Model: We assume that the communication links experience a Rayleigh distributed fast fading with variance equal to 1, e.g., see [30]–[32]. In particular, the fading power of a link between any two nodes remains constant for the transmit duration of T (i.e., phases I and II). The link then experiences a new realization of the exponential channel power in the next transmit interval. However, we note that our model can be easily extended to generalized fading models. Furthermore, in case the transmission links are blocked by objects, the path-loss exponent is assumed to be α_N; otherwise, for links in LOS, the path-loss exponent is assumed to be α_L. As a result, the received power at a device located at a distance r_j from the transmitter j is given as: $P_r = P_j h_j K r_j^{-\alpha_i}$, where K is the path-loss coefficient, P_j is the transmit power from transmitter j, and $i \in \{L, N\}$ depending on if the communication link is in LOS or nonline-of-sight (NLOS). Furthermore, h_j denotes the channel gain over the link from transmitter j and the receiver.

Outage Model: We assume long packet communication, where a device is said to be in outage if the transmission rate exceeds the instantaneous channel capacity, and it is considered successful otherwise. Recall that a URLLC system operates with a strict packet deadline. Accordingly, if a device has not received a given packet by the end of phase II, the packet is dropped and the device moves to the reception of the next packet. In other words, a device is in outage if the received SNR is lower than a threshold imposed by the channel capacity. We denote the SNR thresholds for phases I and II γ_1 and γ_2 as functions of the time partitioning parameter β, as

$$\gamma_1(\beta) = 2^{\frac{R_1}{W}} - 1 = 2^{\frac{b}{\beta T W}} - 1 \tag{3}$$

$$\gamma_2(\beta) = 2^{\frac{R_2}{W}} - 1 = 2^{\frac{b}{(1-\beta)TW}} - 1. \tag{4}$$

III. Coverage Probability and Frame Design

In this section, first we derive the SNR coverage probability of a device located at a distance r from the controller in phase I. Then, given that a device is in outage in the broadcast phase, we derive the SNR coverage probability in phase II. Finally, we use the two results to characterize the overall probability that a device is in coverage after the two phases.

A. Broadcast Phase (Phase I)

The SNR received by a device located at a distance r_0 from the controller in phase I (averaged over the random blockages) is written as follows:

$$\mathrm{SNR}_1(r_0) = \mathcal{P}_B(r_0)\mathrm{SNR}_N(r_0) + (1-\mathcal{P}_B(r_0))\mathrm{SNR}_L(r_0) \tag{5}$$

where based on blockage probability in (2), the first and the second terms in (5) represent the SNR for when the controller-device link is, respectively, in NLOS and LOS state. As a result, the SNR coverage probability can be derived as [33]

$$\begin{aligned}\mathcal{P}_{C1}(r_0,\gamma_1) &= \mathbb{P}(\mathrm{SNR}_1(r_0) \geq \gamma_1)\\ &= \mathbb{P}\left(\mathcal{P}_B\frac{P_0 K h_0 r_0^{-\alpha_N}}{\sigma^2} + (1-\mathcal{P}_B)\frac{P_0 K h_0 r_0^{-\alpha_L}}{\sigma^2} \geq \gamma_1\right)\\ &= \mathbb{P}\left(h_0 \geq \frac{\gamma_1\sigma^2}{P_0 K\left(\mathcal{P}_B r_0^{-\alpha_N} + (1-\mathcal{P}_B) r_0^{-\alpha_L}\right)}\right)\\ &\overset{(a)}{=} \left[\exp\left(\frac{-\gamma_1\sigma^2}{P_0 K\left(\mathcal{P}_B r_0^{-\alpha_N} + (1-\mathcal{P}_B) r_0^{-\alpha_L}\right)}\right)\right]\end{aligned} \tag{6}$$

where P_0 is the transmit power at the central controller and h_0 denotes the channel gain between the central controller and the receiver. In (6), step *(a)* follows from the exponential distribution of the channel gain h_0. Then, the point process ϕ_1 of the locations of the devices under coverage after phase I has an intensity of $\lambda\mathcal{P}_{C1}(r,\gamma_1)$ at distance r from the controller.

B. Relaying Phase (Phase II)

Next, let us characterize the SNR performance of the second phase for two cases: 1) cooperative transmission: where a device in outage receives retransmitted signals from all the devices in ϕ_1 and 2) nearest-relay transmission: where the devices in outage receive services from the device which is nearest to it in ϕ_1. In particular, the nearest-relay transmission provides a simple lower bound for the cooperative transmission case.

1) Full Coordination: For cooperative transmission, the SNR at the test device located at r_0 is given by

$$\mathrm{SNR}_2(r_0) = \frac{h_0 S_0 + S_T'}{\sigma^2} \tag{7}$$

where

$$S_0 = K P_0\left(\mathcal{P}_B(r_0) r_0^{-\alpha_N} + (1-\mathcal{P}_B(r_0)) r_0^{-\alpha_L}\right)$$
$$S_T' = \sum_{k\in\mathcal{R}} K P_k h_k\left(\mathcal{P}_B(r_k) r_k^{-\alpha_N} + (1-\mathcal{P}_B(r_k)) r_k^{-\alpha_L}\right).$$

Authorized licensed use limited to: CEA GRENOBLE. Downloaded on October 13,2022 at 10:28:49 UTC from IEEE Xplore. Restrictions apply.

The first expression corresponds to the transmission from the controller and second expression corresponds to the transmission from the devices under coverage in phase I.

Lemma 2: The cumulative density function (CDF) of S'_R is calculated as

$$F_{S'_T}(x) = \frac{1}{2} - \frac{1}{\pi}\int_0^\infty \frac{\mathcal{I}\Big[\exp(-itx)\phi_{S'_T}(t)\Big]}{t}dt \tag{8}$$

where $\mathcal{I}(z) = ([z - z^*]/[2i])$, and $\phi_{S'_T}(t)$ is the characteristic function of S'_T.

Proof: See Appendix A. ■

Before proceeding, let us note that

$$\begin{aligned} f_{S'_T}(x) &= \frac{d}{dx}\Big(1 - F_{S'_T}(x)\Big) \\ &= \frac{1}{\pi}\int_0^\infty \mathcal{R}(\exp(-itx)\phi_I(t))dt \end{aligned}$$

where $\mathcal{R}(z) = ([z + z^*]/[2])$. Now, we have

$$\begin{aligned} &\mathbb{P}\left(\sum_{j\in\mathcal{R}} P_j h_j\Big(\mathcal{P}_B(r_j)r_j^{-\alpha_N} + (1-\mathcal{P}_B(r_j))r_j^{-\alpha_L}\Big) \le \frac{\gamma_2\sigma^2}{K}\right) \\ &= F_{S'_T}\left(\frac{\gamma_2\sigma^2}{K}\right). \end{aligned} \tag{9}$$

Theorem 1: The coverage probability of the test device to be in coverage in Phase 2 is given by

$$\begin{aligned} \mathcal{P}_{C2}(r_0) = \exp\frac{\gamma_2\sigma^2}{S_0}&\int_{\gamma_2\sigma^2-\gamma_1\sigma^2}^{\gamma_2\sigma^2}\exp\frac{-x}{S_0}f_{S'_R}(x)dx \\ &- \exp\frac{\gamma_1\sigma^2}{S_0}\Big(F_{S'_T}(\gamma_2\sigma^2) - F_{S'_T}((\gamma_2-\gamma_1)\sigma^2)\Big) \\ &+ \left(1 - \exp\left(-\frac{\gamma_1\sigma^2}{S_0}\right)\right)\Big(1 - F_{S'_R}(\gamma_2\sigma^2)\Big) \end{aligned} \tag{10}$$

where $\mathcal{A}_R = KP_N(\mathcal{P}_B(y)y^{-\alpha_N} + (1-\mathcal{P}_B(y))y^{-\alpha_L})$.

Proof: See Appendix B. ■

2) Nearest-Relay Transmission: Next, we analyze the SNR coverage probability in phase II for a device i under outage in phase I, which receives data from its closest device under coverage after phase I. Let us denote with r_2 the distance between the device i and its relay in the phase II; then, the SNR at the test device located at r_0 is given by

$$\mathrm{SNR}_2(r_0) = \frac{h_2 S_2}{\sigma^2} \tag{11}$$

where

$$S_2 = KP_2\Big(\mathcal{P}_B(r_2)r_2^{-\alpha_N} + (1-\mathcal{P}_B(r_2))r_2^{-\alpha_L}\Big).$$

For evaluating the above, first, we characterize the probability density function (pdf) of r_2 in the following Lemma.

Lemma 3: The cumulative density function (CDF) of the distance of the nearest point of ϕ_1 from device i is given by

$$F_{r_2}(r) = \begin{cases} 1 - \exp\Big(-\lambda\int_{r_0-r}^{r_0+r}\int_0^{\sqrt{r^2-(x-r_0)^2}} \\ \mathcal{P}_{C1}\Big(\sqrt{x^2+y^2}, \gamma_1\Big)dydx\Big); \quad 0 \le r_2 \le R - r_0 \\ 1 - \exp(-A_1(r) - A_2(r)); \quad R - r_0 < r_2 \le R + r_0 \\ 1; \quad \text{otherwise} \end{cases}$$

where

$$A_1(r) = \int_{r_0-r}^{x_r}\int_0^{\sqrt{r^2-(x-r_0)^2}} \mathcal{P}_{C1}\left(\sqrt{x^2+y^2}, \gamma_1\right)dydx$$

$$A_2(r) = \int_{x_r}^{R}\int_0^{\sqrt{R^2-x^2}} \mathcal{P}_{C1}\left(\sqrt{x^2+y^2}, \gamma_1\right)dydx$$

and

$$x_r = \frac{R^2 - r^2 + r_0^2}{2r_0}.$$

Consequently, the pdf of the nearest point of ϕ_1 from the test device i is given by (12), shown at the bottom of the page, where

$$\begin{aligned} T_1(r) = \lambda\Bigg[\exp\Bigg(&-\lambda\int_{r_0-r}^{x_r}\int_0^{\sqrt{r^2-(x-r_0)^2}} \mathcal{P}_{C1}\left(\sqrt{x^2+y^2}, \gamma_1\right)dydx \\ &- \lambda\int_{x_r}^{R}\int_0^{\sqrt{R^2-x^2}} \mathcal{P}_{C1}\left(\sqrt{x^2+y^2}, \gamma_1\right)dydx\Bigg)\Bigg] \end{aligned}$$

$$\begin{aligned} T_2(r) = &\int_0^{\sqrt{r^2-(x_r-r_0)^2}} \mathcal{P}_{C1}\left(\sqrt{{x_r}^2+y^2}, \gamma_1\right)dy\frac{-r}{r_0} + \\ &+ \int_{r_0-r}^{x_r} \mathcal{P}_{C1}\left(\sqrt{x^2+r^2-(x-r_0)^2}, \gamma_1\right)\frac{r}{\sqrt{r^2-(x-r_0)^2}}dx \\ &+ \frac{r}{r_0}\int_0^{\sqrt{R^2-x_r^2}} \mathcal{P}_{C1}\left(\sqrt{x_r^2+y^2}, \gamma_1\right)dy. \end{aligned}$$

Proof: See Appendix C. ■

Lemma 4: Finally, the SNR coverage probability of the test device in the second phase is given by

$$\begin{aligned} \mathcal{P}_{C2}(r_2, \gamma_2) &= \mathbb{P}(\mathrm{SNR}_2(r_0) \ge \gamma_2) \\ &= \mathbb{P}(\mathcal{P}_B(r)\mathrm{SNR}_N(r) + (1-\mathcal{P}_B(r))\mathrm{SNR}_L(r) \ge \gamma_2) \end{aligned}$$

$$f_{r_2}(r) = \begin{cases} 2\lambda\exp\Big(-2\lambda\int_{r_0-r}^{r_0+r}\int_0^{\sqrt{r^2-(x-r_0)^2}}\mathcal{P}_{C1}\Big(\sqrt{x^2+y^2}, \gamma_1\Big)dydx\Big)\Big[\int_{r_0-r}^{r_0+r}\Big(\mathcal{P}_{C1}(x^2 + (r^2-(x-r_0)^2), \gamma_1)\frac{r}{\sqrt{r^2-(x-r_0)^2}}\Big)dx\Big] \\ \quad 0 \le r_2 \le R - r_0 \\ T_1(r)\cdot T_2(r); \quad R - r_0 < r_2 \le R + r_0 \\ 0; \quad \text{otherwise} \end{cases} \tag{12}$$

Authorized licensed use limited to: CEA GRENOBLE. Downloaded on October 13,2022 at 10:28:49 UTC from IEEE Xplore. Restrictions apply.

$$= \mathbb{P}\left(\mathcal{P}_B \frac{P_2 K h_2 r_2^{-\alpha_N}}{\sigma^2} + (1-\mathcal{P}_B)\frac{P_2 K h_2 r_2^{-\alpha_L}}{\sigma^2} \geq \gamma_2\right)$$
$$= \mathbb{P}\left(h_2 \geq \frac{\gamma_2 \sigma^2}{P_2 K\left(\mathcal{P}_B r_2^{-\alpha_N} + (1-\mathcal{P}_B) r_2^{-\alpha_L}\right)}\right)$$
$$\overset{(a)}{=} \mathbb{E}_{r_2}\left[\exp\left(\frac{-\gamma_2\sigma^2}{P_0 K\left(\mathcal{P}_B r_2^{-\alpha_N} + (1-\mathcal{P}_B) r_2^{-\alpha_L}\right)}\right)\right] \quad (13)$$

where the expectation is taken with respect to r_2, as given in Lemma 3.

3) Overall Coverage Probability: Using the theorem of total probability, and due to the independence of the random events of failure in phases I and II, the overall coverage probability after the two phases can be written as follows:

$$\mathcal{P}_C(r_0, \gamma_1, \gamma_2) = \mathcal{P}_{C1}(r_0, \gamma_1) + \mathcal{P}_{C2}(r_0, \gamma_2) - \mathcal{P}_{C1}(r_0, \gamma_1)\cdot \mathcal{P}_{C2}(r_0, \gamma_2). \quad (14)$$

Impact of Blockage Speed: In the above development, we have assumed an agile blockage model, wherein a given transmission event between two nodes (a transmitter and a receiver) experiences several blockage events. Accordingly, the coverage probability is defined as the probability that the received power averaged over blockages is larger than a threshold (γ_1 in phase 1 and γ_2 in phase 2).

On the contrary, in case the speed of the blockages is low, a link remains in the same visibility state (whether LOS or NLOS) throughout the transmit duration. Let us analyze the same for the case of nearest-relay transmission. Accordingly, the coverage probability of phase 1 is given as

$$\mathcal{P}_{C1}(r_0, \gamma_1) = \mathcal{P}_B(r_0)\mathbb{P}(\mathrm{SNR}_{N1}(r_0) \geq \gamma_1 \mid N) + (1-\mathcal{P}_B)(\mathrm{SNR}_{L1}(r_0) \geq \gamma_1 \mid L)$$
$$= \mathcal{P}_B(r_0)\mathbb{P}\left(\frac{P_0 K h_0 r_0^{-\alpha_N}}{\sigma^2} \geq \gamma_1\right) + (1-\mathcal{P}_B(r_0))\left(\frac{P_0 K h_0 r_0^{-\alpha_L}}{\sigma^2} \geq \gamma_1\right)$$
$$= \mathcal{P}_B(r_0)\exp\left(\frac{-\gamma_1\sigma^2}{P_0 K r_0^{-\alpha_N}}\right) + (1-\mathcal{P}_B(r_0))\exp\left(\frac{-\gamma_1\sigma^2}{P_0 K r_0^{-\alpha_L}}\right).$$

Then, the SNR coverage probability in the second phase with low-mobility blockages is given by

$$\mathcal{P}_{C2}(r_0, \gamma_2) = \mathbb{E}_{r_2}\left[\mathcal{P}_B(r_2)\exp\left(\frac{-\gamma_1\sigma^2}{P_2 K r_2^{-\alpha_N}}\right) + (1-\mathcal{P}_B(r_2))\exp\left(\frac{-\gamma_1\sigma^2}{P_2 K r_2^{-\alpha_L}}\right)\right].$$

Optimal Cooperative Frame Design: To optimize the coverage, it is important to study the optimal time division between the two phases described in Section II. When a small share of the total time T is allotted to phase I, only few devices that experience a high quality link are able to correctly receive the transmitted data, which limits the number of available relays in phase II. Whereas, in case a large amount of time is allotted to phase I, this leads to a high number of devices successfully decoding the transmissions in phase I but it requires to use a very high data rate in phase II, to relay the intended message. Therefore, we analyze the optimal time partitioning parameter $\beta \in [0, 1]$ that minimizes the total probability of outage in cycle time T.

Then, the problem of designing the optimal β to optimize the system performance can be mathematically stated as

$$\beta^* = \underset{\beta\in[0;1]}{\arg\min}\ \mathcal{P}_{\mathrm{out}}(\beta). \quad (15)$$

The outage probability $\mathcal{P}_{\mathrm{out}}(\beta)$ is defined as follows:

$$\mathcal{P}_{\mathrm{out}}(\beta) = 1 - \int_0^{2\pi}\int_0^R \mathcal{P}_C(r, \gamma_1(\beta), \gamma_2(\beta)) f_{r,\theta}(r,\theta)\, dr d\theta$$

where $f_{r,\theta}$ is the uniform distribution of the location of the test device, in which r refers to the distance of the device from the central controller and θ denotes the angle between the x-axis and the line joining the controller and the device.

IV. Numerical Results and Discussion

Now, we assess the performance of the cooperative communication protocol analyzed in this article, with respect to the number of devices, density of the random blockages, transmit power, and the time splitting factor β. In particular, we tune the blockage density using parameter λ_P, i.e., the density of the parent PPP from which the MHCP is derived.[3] We assume a circular deployment area with dimension $R = 50$ m, a system bandwidth $W = 1$ MHz, carrier frequency equals to 3.5 GHz, $\alpha_L = 2$, and $\alpha_N = 4$. The blockages are considered to be of radius $R_B = 0.5$ m. Unless otherwise specified, we assume $P_0 = 23$ dBm and $P_N = 20$ dBm.

A. Effect of the Data Size

In Fig. 3, we plot the outage probability for the three different schemes: 1) broadcast only (by setting $\beta = 1$); 2) full coordination, i.e., all the devices in Φ_1 transmit to the devices in outage; and 3) the nearest relay scheme. We note that for lower data sizes, cooperative transmission (either nearest relay or full coordination) significantly increases the outage performance (e.g., by more than five orders of magnitude for 11 bits). Interestingly, the nearest-relay transmission scheme provides a close upper bound for the full-coordination scheme. This bound becomes tighter for higher data size. Thus, for a device in Φ_1', i.e., a device in outage at the end of phase I, the gain with full cooperation is only marginal as compared to the nearest-relay cooperative transmission. Furthermore, due to the tight upper bound, the insights for the full cooperation case naturally follows from the nearest-relay transmission, which we consider for the rest of the results.

[3]For the values of R_B considered in this article, the values of λ_B and λ_P do not differ considerably. In particular, as λ_P varies from 1e-5 m^{-2} to 1e-1 m^{-2}, the value of λ_B changes from 1e-5 m^{-2} to 0.0985 m^{-2}. Accordingly, λ_P is an accurate estimation of the actual blockage density in the network. In fact, for $R_B \leq 1$, $\lambda_B \approx \lambda_P$ up to $\lambda_P \leq 1e-1$ m^{-2}.

Authorized licensed use limited to: CEA GRENOBLE. Downloaded on October 13,2022 at 10:28:49 UTC from IEEE Xplore. Restrictions apply.

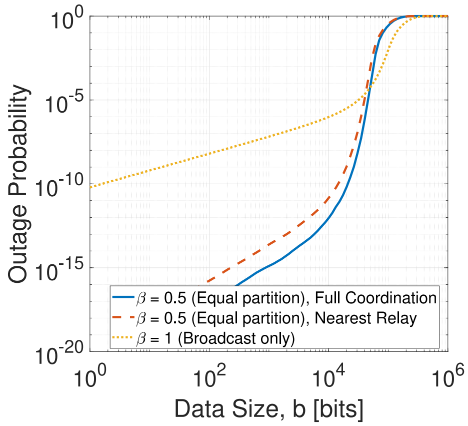

Fig. 3. Outage probability versus data size for different cooperation strategies, for $\lambda = 0.01$ m^{-2}.

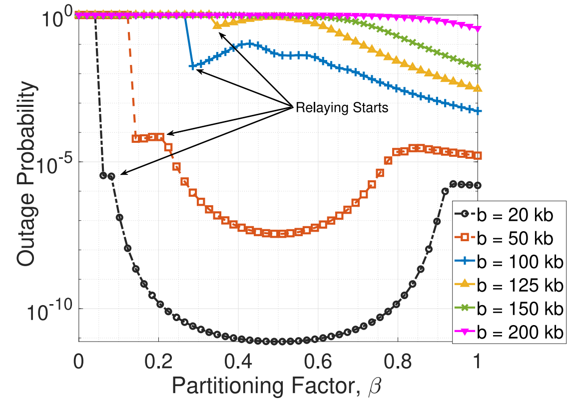

Fig. 5. Outage probability versus the resource partitioning factor for different values of data size, b. $\lambda = \lambda_P = 1e - 2$ m^{-2}.

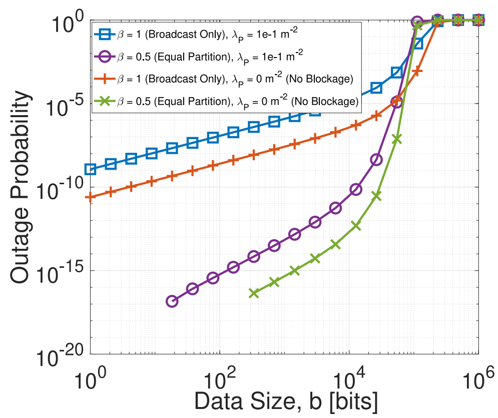

Fig. 4. Outage probability versus data size for different partitioning factors and blockage densities, for $\lambda = 0.01$ m^{-2} and $\lambda_P = 0.01$ m^{-2}.

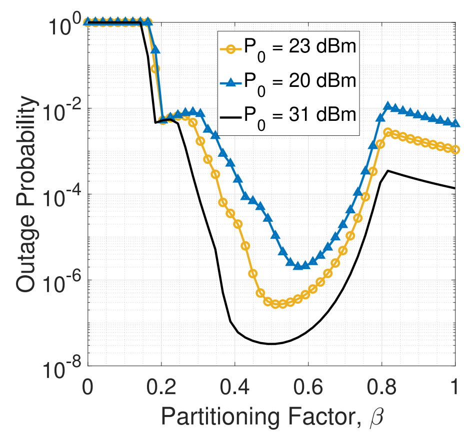

Fig. 6. Outage probability versus resource partitioning factor for different values of controller power. $\lambda_P = 1e - 1$ m^{-2} and $\lambda = 5e - 2$ m^{-2}.

In Fig. 4, we note that regardless of the value of β and b, the presence of blockages increases the outage probability by two orders in magnitude. This highlights the importance of taking the blockages into consideration for such URLLC applications, even in the sub-6-GHz band. As expected, the outage increases with increasing data size.

Interestingly, when the packet size is too large (e.g., larger that 100 kb in Fig. 4), the equal partitioning strategy ($\beta = 0.5$) performs poorer than the broadcast strategy ($\beta = 1$). This is due to the fact that for a large packet size, i.e., high transmission rate, the broadcast phase with $\beta = 0.5$ fails to successfully deliver the packet to large enough number of devices, which, in turn, diminishes the benefits of allocating the remaining 0.5 of the total time to the relaying phase. As a result, for large data sizes, the outage of the equal partitioning scheme is higher than the broadcast only strategy.

This point is further highlighted in Fig. 5, where we plot the outage probability with respect to the resource partitioning factor for different values of data size, b. Evidently, based on the size of the data packet, the trend of the outage probability with respect to β follows one of the following. First, for small packet sizes (e.g., $b = 20$ kb or 50 kb), the two-phase strategy with relaying provides a better outage probability than the single-phase broadcast strategy. Therefore, optimizing the partitioning factor β has a meaningful impact on the outage probability, which reaches an optimal value near $\beta = 0.5$ with equal partition of resources. Second, for large packet sizes (e.g., $b = 100$ kb and more), the gain of the two-phase strategy is marginalized, resulting in optimal partitioning of $\beta = 1$. In particular, we see that for $b = 150$ kb and $b = 200$ kb, the outage monotonically decreases with β, indicating that it is directly dependent on the resources allotted to phase I.

It should be noted that for intermediate data sizes, e.g., 100 kb and 125 kb, we observe an initial decrease in the outage probability with the onset of relaying. This is followed by an increase in the outage. Indeed, for these data sizes, although an increased number of devices get coverage in the broadcast phase with an increase in β, a reduced amount of resources are available for successful relaying of a file with large data size. After a threshold on β, the outage reaches the regime where the outage decreases with increasing the length of phase I.

B. Effect of the Controller Power

In Fig. 6, we plot the outage probability with respect to β for different values of controller transmit power in a dense blocking environment ($\lambda_P = 1e - 1$ m^{-2}). We observe that the controller power has a significant effect on the optimal value of β. In particular, as the transmit power of the controller

Authorized licensed use limited to: CEA GRENOBLE. Downloaded on October 13,2022 at 10:28:49 UTC from IEEE Xplore. Restrictions apply.

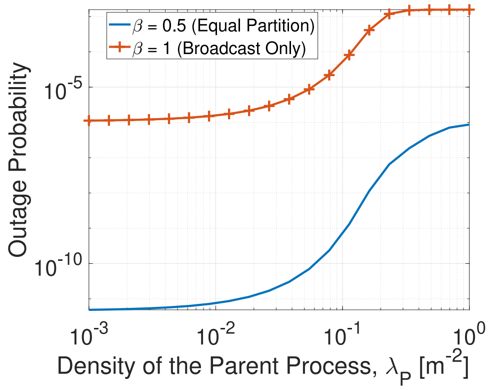

Fig. 7. Outage probability versus blockage density for two values of β. $b = 20$ kb and $\lambda = 0.01$ m^{-2}.

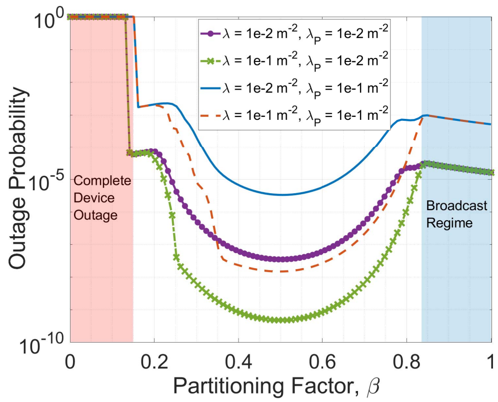

Fig. 8. Outage probability versus partitioning factor for different device and blockage densities.

decreases, the optimal value of β shifts toward 1. This indicates that for a lower transmit power of the controller, a larger amount of resources need to be allotted to the broadcast phase so as to minimize the outage. Naturally, for lower P_0, we observe a higher value of outage.

C. Effect of the Device and Blockage Densities

In Fig. 7, we plot the outage probability as a function of λ_P with $b = 20$ kb and $\lambda = 1e-2$ m^{-2}. As expected, the outage increases with increasing λ_P with relatively flat regions for $\lambda_P \leq 5e-3$ m^{-2} and $\lambda_P \geq 5e-1$ m^{-2}. The former region is the case where there are no blockages in the area (recall that the area has a radius of $R = 50$ m), whereas the later represents the case where the area is saturated with blockages. That is, due to the repulsive nature of the MHCP, increasing λ_P beyond $5e-1$ m^{-2} does not increase the number of blockages for a fixed area. We observe that for any value of blockage density, a simple equal partition policy outperforms the broadcast-only strategy.

In Fig. 8, we plot the outage probability with respect to the resource partitioning factor for different values of device and blockage densities. Foremost, we note the complete device outage region shown in the red shaded region. This region corresponds to the range of β where it is not possible to provide reliable coverage to the test device. Moreover, we observe that an increase in the density of the devices (which increases the number of potential relays and reduces the distance between the test device and the potential relay) decreases the outage probability. This is the case for fixed packet size b, where by increasing the number of devices in the network, the transmission rate remains fixed, while the potential gain from the relaying phase increases. In fact, for both $\lambda_P = 1e-2$ m^{-2} and $\lambda_P = 1e-1$ m^{-2}, a tenfold increase in the device density decreases the outage by two orders in magnitude.

For high values of β, the resources available to the relays in phase II are less for facilitating a successful transmission. In that case, the test-node enters the *broadcast regime* (shown by the blue shaded region in Fig. 8), in which the outage depends only on phase I transmission. In this phase, an increase in β decreases the outage due to more resources allotted to phase I. At $\beta = 1$, the outage value reaches the same as a "broadcast-only" transmission scheme.

We study this interplay of λ and λ_P, and their effect on the optimal β and outage in the next section.

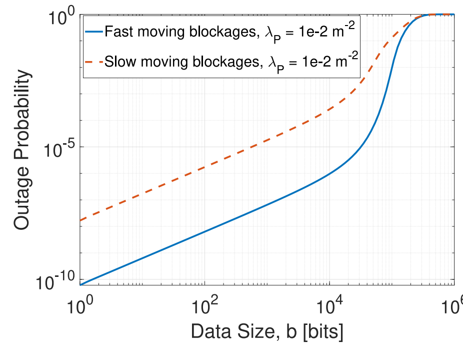

Fig. 9. Impact of blockage speeds on the outage probability with $\beta = 0.5$.

D. Impact of the Speed of Blockages

We compare the outage probabilities for the case of low-mobility blockages with that of high-speed blockages in Fig. 9, with $\lambda_P = 0.01$ m^{-2}. We observe that for the case when the link visibility status does not change during the transmission, and accordingly, a fraction of the links always remains in the NLOS state, the outage of the devices is higher.

E. Trends in the Optimal Partitioning Factor

In Fig. 10, we plot the optimal value of the partitioning factor as a function of the device density for different values of data size and blockage density. In all the cases, we see that for a very low device density, the optimal β is 1, due to the limited number of potential relays and the resulting gain of the relaying phase. For a high blockage density, i.e., $\lambda_P = 1e-1$ m^{-2}, we observe an interesting phenomenon: as the device density increases and the nearest device comes closer to the test device, the system has to balance between two contending behaviors: 1) higher β facilitating a larger number of relays close to the test device, albeit decreasing the resources available to them in the relay phase or 2) lower β thereby giving an increased amount of resources to a lower number of relays. The balance between these two behaviors is

Authorized licensed use limited to: CEA GRENOBLE. Downloaded on October 13,2022 at 10:28:49 UTC from IEEE Xplore. Restrictions apply.

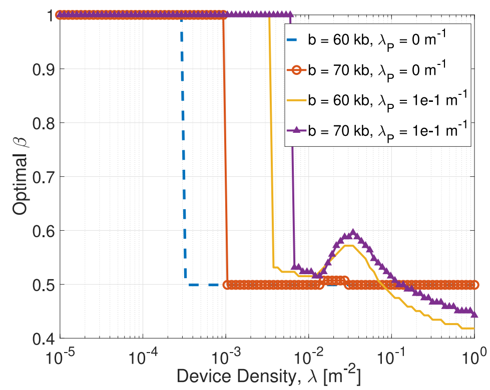

Fig. 10. Optimal value of the partitioning factor versus the device density for fixed data size.

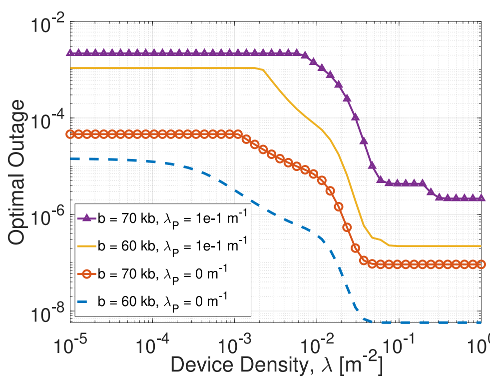

Fig. 11. Optimal outage probability with fixed data size.

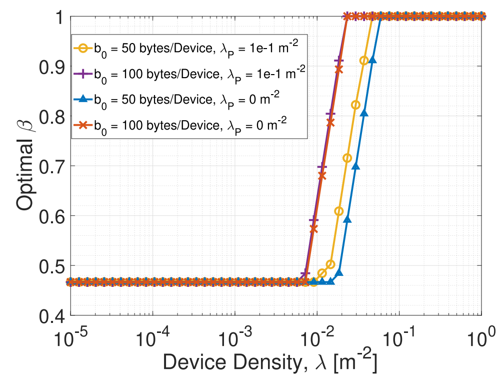

Fig. 12. Optimal value of partitioning factor versus the device density when the data size depends on the number of devices.

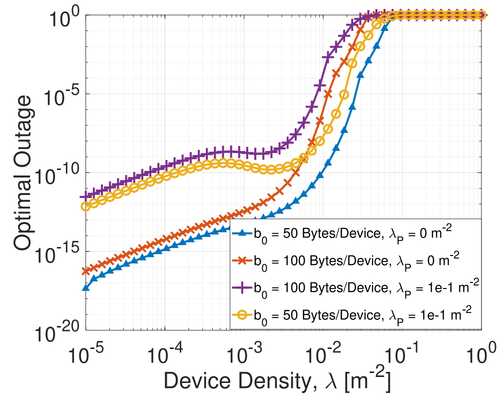

Fig. 13. Optimal outage probability with device dependent data size.

nontrivial and hence, we see a nonmonotonous nature for the optimal β for high blockage densities.

In the absence of blockages, this nontrivial behavior is limited. In fact, for no blockages, the optimal β is 1 as long as very few devices are present in the network, and switches to the equal partition ($\beta = 0.5$) option as soon as enough potential relays are available (e.g., when $\lambda \geq 1e-3$ m^{-2}). However, around $\lambda = 5e-2$ the optimal β shows a slight increase before settling back to 0.5.

The corresponding optimal outage values are shown in Fig. 11. In the broadcast regime (see also Fig. 10), the optimal outage is constant up till a certain λ for a given b and λ_P, for which a cooperative transmission is beneficial. For a large value of device density (e.g., $\lambda \geq 5e-1$ m^{-2}), increasing λ does not bring the nearest device significantly closer to the test device and hence, the optimal outage saturates.

Finally, in Fig. 12, we plot the optimal value of β when the data size is a function of the number of devices in the network. In this case, the data size is $2\pi R^2 b_0$, where b_0 denotes the data size per device. Unlike the case of fixed data size, in this case, the optimal value of the resource partitioning factor has a monotonous trend with the number of devices in the factory. In fact, for very high density of the devices, the optimal β reaches 1 indicating that resource sharing deteriorates the outage. This is due to the fact that high device density corresponds to a very high data size that needs to be transmitted (as the case related to blue plot in Fig. 5).

The corresponding optimal outage values are presented in Fig. 13. In the absence of blockages, the optimal outage increases with the device density due to the corresponding increase in the data size. However, for a heavy blockage environment ($\lambda_P = 1e-1$ m^{-2}), the trend of the optimal outage is not monotonic with the increase of the device density. Near $\lambda = 1e-3$ m^{-2}, the outage slightly decreases before increasing again. This highlights the nontrivial effect of increasing the devices in the network, i.e., a large number of devices corresponds to a large number of potential relays, which enhances the performance of the cooperative transmission. However, with an increasing number of devices, the file sizes increase, which limits the coverage probability.

Here, we note that a further partitioning of the total transmit time into multiple relay phases (instead of 1, as considered in this article) may improve the coverage even further. Additionally, considering a fully cooperative system where a device in outage can receive services from all the relays in the second phase is an interesting research problem. We will investigate these aspects of the network in a future work.

V. Conclusion

We have investigated an industry automation scenario where a central node communicates with wireless devices on the factory floor. First, we have shown that it is imperative to take into account the physical blockages, since they increase the outage probability by about two orders of magnitude. Then,

Authorized licensed use limited to: CEA GRENOBLE. Downloaded on October 13,2022 at 10:28:49 UTC from IEEE Xplore. Restrictions apply.

to mitigate the service outage due to blockages or poor channel conditions, we propose and characterize a resource partitioning scheme in which the communication resources are divided into broadcast and relay phases so as to facilitate successful transmission of the intended data. Our study highlights that when the data size depends on the number of users, the optimal resource partitioning factor is tightly coupled with the device density. In that case, the optimal solution is to increase the length of the phase I with the device density. Whereas, when the data size is fixed, the optimal resource partitioning factor shows a nontrivial behavior due to the contending effects of increasing β, which increases the relay density, but also decreases the resources available to these relays.

APPENDIX A
PROOF OF LEMMA 2

Note that S'_T is a random variable consisting of a sum of pointwise functions of the thinned (with respect to the coverage probability in the first phase) PPP. Let us calculate the characteristic function of this random variable

$$
\begin{aligned}
\phi_{S'_T}(t) &= \mathbb{E}\big[\exp(itI)\big]\\
&= \mathbb{E}\left[\exp\left(it\sum_{j\in\mathcal{R}} P_j h_j\Big(\mathcal{P}_B(r_j)r_j^{-\alpha_N} + (1-\mathcal{P}_B(r_j))r_j^{-\alpha_L}\Big)\right)\right]\\
&\overset{(a)}{=} \mathbb{E}\left[\prod_{j\in\mathcal{R}} \exp\Big(it\Big(P_j h_j\Big(\mathcal{P}_B(r_j)r_j^{-\alpha_N} + (1-\mathcal{P}_B(r_j))r_j^{-\alpha_L}\Big)\Big)\Big)\right]\\
&\overset{(b)}{=} \mathbb{E}\left[\prod_{j\in\mathcal{R}} \frac{1}{1-it\Big(P_j\Big(\mathcal{P}_B(r_j)r_j^{-\alpha_N} + (1-\mathcal{P}_B(r_j))r_j^{-\alpha_L}\Big)\Big)}\right]\\
&\overset{(c)}{=} \exp\Bigg(-2\pi\int_0^R 1-\\
&\qquad \left(\frac{1}{1-it\big(P_j\big(\mathcal{P}_B(x)x^{-\alpha_N} + (1-\mathcal{P}_B(x))x^{-\alpha_L}\big)\big)}\right)\lambda\mathcal{P}_{C1}(x)dx\Bigg).
\end{aligned}
\tag{16}
$$

Here, (a) is from the fact that an exponential of sum is equal to product of exponential. In (b), we take the Laplace transform with respect to independent identically distributed (i.i.d.) random variables h_j. As all h_j are identically distributed, the resulting terms are of the same form. The step (c) follows from Campbells theorem. The CDF is directly related to the characteristic function. Using the Gil–Pelaez inversion theorem, we have

$$
F_{S'_T}(x) = \frac{1}{2} - \frac{1}{\pi}\int_0^\infty \frac{\mathcal{I}\big[\exp(-itx)\phi_I(t)\big]}{t}dt \tag{17}
$$

where $\mathcal{I}(z) = \frac{z-z^*}{2i}$ is the imaginary part of z.

APPENDIX B
PROOF OF THEOREM 1

Let

$$
\begin{aligned}
S_T &= \sum_{j\in\mathcal{R}} P_j K\Big(\mathcal{P}_B(r_j)r_j^{-\alpha_N} + (1-\mathcal{P}_B(r_j))r_j^{-\alpha_L}\Big)\\
\mathcal{P}_{C2}(r_0,\gamma_1,\gamma_2) &= \mathbb{P}(\mathrm{SNR}_2(r_0) \geq \gamma_2 \cap \mathrm{SNR}_1(r_0) \leq \gamma_1)\\
&= \mathbb{P}\Big(P_0 h_0\Big(\mathcal{P}_B(r_0)r_0^{-\alpha_N} + (1-\mathcal{P}_B(r_0))r_0^{-\alpha_L}\Big)\\
&\quad + \sum_{j\in\mathcal{R}} P_j h_j\Big(\mathcal{P}_B(r_j)r_j^{-\alpha_N} + (1-\mathcal{P}_B(r_j))r_j^{-\alpha_L}\Big)\\
&\geq \frac{\gamma_2\sigma^2}{K} \cap \Big(\mathcal{P}_B(r_0)P_0 K h_0 r_0^{-\alpha_N}\\
&\quad + (1-\mathcal{P}_B(r_0))P_0 K h_0 r_0^{-\alpha_L}\Big).\\
&\leq \gamma_1\sigma^2\Big)\\
&= \mathbb{P}\left(h_0 \geq \frac{\gamma_2\sigma^2 - S'_T}{S_0} \cap h_0 \leq \frac{\gamma_1\sigma^2}{S_0}\right)\\
&= \mathbb{P}\left(\frac{\gamma_2\sigma^2 - S'_T}{S_0} \leq h_0 \leq \frac{\gamma_1\sigma^2}{S_0} \cap\right.\\
&\quad \left. 0 \leq \frac{\gamma_2\sigma^2 - S'_T}{S_0} \leq \frac{\gamma_1\sigma^2}{S_0}\right)\\
&\quad \mathbb{P}\left(h_0 \leq \frac{\gamma_1\sigma^2}{S_0}\right)\cdot\mathbb{P}\left(\frac{\gamma_2\sigma^2 - S'_T}{S_0} \leq 0\right)\\
&= \int_{\gamma_2\sigma^2-\gamma_1\sigma^2}^{\gamma_2\sigma^2}\left(\exp\frac{\gamma_2\sigma^2 - x}{S_0} - \exp\frac{\gamma_1\sigma^2}{S_0}\right)f_{S'_R}(x)dx\\
&\quad + \left(1-\exp\left(-\frac{\gamma_1\sigma^2}{S_0}\right)\right)\Big(1-F_{S'_R}(\gamma_2\sigma^2)\Big).
\end{aligned}
$$

Simplifying the above completes the proof.

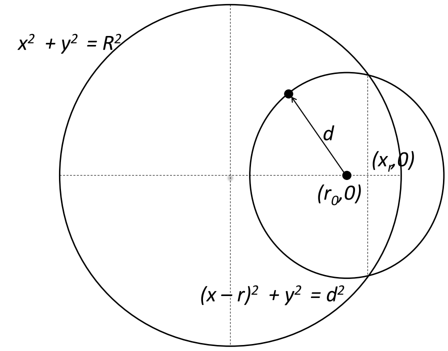

Fig. 14. Illustration for the calculation of pdf of the nearest relay.

APPENDIX C
PROOF OF LEMMA 3

Let the nearest point of the process ϕ_1 be at a distance $r_2 = r$ from the device i. This implies that in Fig. 14, there are no points of ϕ_1 within the intersection of the two circles $\mathcal{A}_{r_0,r} = \mathcal{B}(r_0, r_2) \cap \mathcal{B}(0, R)$. Accordingly, the CDF of r_2 is derived as follows.

Case 1 ($r_2 \leq R - r_0$): Here, the circle $\mathcal{B}(r_0, r_2)$ lies completely inside the circle $\mathcal{B}(0, R)$. Accordingly, the CDF is derived as

$$
\begin{aligned}
F_{r_2}(r) &= \mathbb{P}(r_2 \leq r)\\
&= 1 - \exp\left(-\lambda\int_{z\in\mathcal{B}(r_0,r)} \mathcal{P}_{C1}(z,\gamma_1)dz\right)\\
&= 1 - \exp\Bigg(-\lambda\int_{r_0-r}^{r_0+r}\int_0^{\sqrt{r^2-(x-r_0)^2}}\\
&\qquad \mathcal{P}_{C1}\left(\sqrt{x^2+y^2},\gamma_1\right)dydx\Bigg).
\end{aligned}
$$

Authorized licensed use limited to: CEA GRENOBLE. Downloaded on October 13,2022 at 10:28:49 UTC from IEEE Xplore. Restrictions apply.

In this case

$$
\begin{aligned}
f_{r_2}(r) &= \frac{d}{dr}F_{r_2}(r) \\
&= \lambda(1-F_{r_2}(r))\left[\int_{r_0-r}^{r_0+r}\left(\frac{d}{dr}\int_0^{\sqrt{r^2-(x-r_0)^2}}\right.\right. \\
&\quad \left.\left.\mathcal{P}_{C1}(x^2+y^2,\gamma_1)dy\right)dx\right] \\
&= \lambda(1-F_{r_2}(r))\left[\int_{r_0-r}^{r_0+r}\right.(\\
&\quad \left.\left.\mathcal{P}_{C1}(x^2+r^2-(x-r_0)^2,\gamma_1)\frac{r}{\sqrt{r^2-(x-r_0)^2}}\right)dx\right].
\end{aligned}
$$

Case 2 ($R-r_0 < r_2 \le R+r_0$): Here, we have to calculate the region of intersection between the two circles. In the Cartesian coordinate system of Fig. 14, the equation of the two circles is as follows: $\mathcal{B}(0,R) \sim x^2+y^2=R^2$ and $\mathcal{B}(r_0,r) \sim (x-r_0)^2+y^2=r^2$. Accordingly, we have

$$
\begin{aligned}
F_{r_2}(r) &= \mathbb{P}(r_2 \le r) = 1-\mathbb{P}(r_2 > r) \\
&= 1-\exp\left(-\int_{z\in\mathcal{A}_{r_0,r}}\lambda\mathcal{P}_{C1}(||z||,\gamma_1)dz\right) \\
&= 1-\exp\left(-\lambda\left(\int_{r_0-r}^{x_r}\int_0^{\sqrt{r^2-(x-r_0)^2}}\mathcal{P}_{C1}\left(\sqrt{x^2+y^2},\gamma_1\right)dydx\right.\right. \\
&\quad \left.\left.+\int_{x_r}^{R}\int_0^{\sqrt{R^2-x^2}}\mathcal{P}_{C1}\left(\sqrt{x^2+y^2},\gamma_1\right)dydx.\right)\right). \qquad (18)
\end{aligned}
$$

Using Leibniz's chain rule, we derive $f_{r_2}(r)$ as follows:

$$
\begin{aligned}
f_{r_2}(r) &= -\frac{d}{dr}F_{r_2}(r) \\
&= -\frac{d}{dr}\exp\left(-2\lambda\left(\int_{r_0-r}^{x_r}\int_0^{\sqrt{r^2-(x-r_0^2)}}\mathcal{P}_{C1}\left(\sqrt{x^2+y^2},\gamma_1\right)dydx\right.\right. \\
&\quad \left.\left.+\int_{x_r}^{R}\int_0^{\sqrt{R^2-x^2}}\mathcal{P}_{C1}\left(\sqrt{x^2+y^2},\gamma_1\right)dydx\right)\right) \\
&= 2\lambda\left[\exp\left(-2\lambda\int_{r_0-r}^{x_r}\int_0^{\sqrt{r^2-(x-r_0^2)}}\mathcal{P}_{C1}\left(\sqrt{x^2+y^2},\gamma_1\right)dydx\right.\right. \\
&\quad \left.\left.-2\lambda\int_{x_r}^{R}\int_0^{\sqrt{R^2-x^2}}\mathcal{P}_{C1}\left(\sqrt{x^2+y^2},\gamma_1\right)dydx\right)\right]. \\
&\quad \left(\frac{d}{dr}A_1(r)+\frac{d}{dr}A_2(r)\right).
\end{aligned}
$$

The derivatives in the above are evaluated as $T_1(r)$ and $T_2(r)$ in the statement of the lemma.

REFERENCES

[1] G. Cena, A. Valenzano, and S. Vitturi, "Hybrid wired/wireless networks for real-time communications," *IEEE Ind. Electron. Mag.*, vol. 2, no. 1, pp. 8–20, Mar. 2008.

[2] *Service Requirements for Cyber-Physical Control Applications in Vertical Domains*, 3GPP Standard TS 22.104, Dec. 2018.

[3] F. Foukalas, P. Pop, F. Theoleyre, C. A. Boano, and C. Buratti, "Dependable wireless industrial IoT networks: Recent advances and open challenges," in *Proc. IEEE Eur. Test Symp. (ETS)*, Baden-Baden, Germany, 2019, pp. 1–10.

[4] V. C. Gungor and G. P. Hancke, "Industrial wireless sensor networks: Challenges, design principles, and technical approaches," *IEEE Trans. Ind. Electron.*, vol. 56, no. 10, pp. 4258–4265, Oct. 2009.

[5] Z. Li, M. A. Uusitalo, H. Shariatmadari, and B. Singh, "5G URLLC: Design challenges and system concepts," in *Proc. 15th Int. Symp. Wireless Commun. Syst. (ISWCS)*, Lisbon, Portugal, 2018, pp. 1–6.

[6] J. Cheng, W. Chen, F. Tao, and C.-L. Lin, "Industrial IoT in 5G environment towards smart manufacturing," *J. Ind. Inf. Integr.*, vol. 10, pp. 10–19, Jun. 2018.

[7] H. Ji, S. Park, J. Yeo, Y. Kim, J. Lee, and B. Shim, "Ultra-reliable and low-latency communications in 5G downlink: Physical layer aspects," *IEEE Wireless Commun.*, vol. 25, no. 3, pp. 124–130, Jun. 2018.

[8] S. Tayeb, S. Latifi, and Y. Kim, "A survey on IoT communication and computation frameworks: An industrial perspective," in *Proc. IEEE 7th Annu. Comput. Commun. Workshop Conf. (CCWC)*, Las Vegas, NV, USA, 2017, pp. 1–6.

[9] J. G. Andrews *et al.*, "What will 5G be?" *IEEE J. Sel. Areas Commun.*, vol. 32, no. 6, pp. 1065–1082, Jun. 2014.

[10] S. W. H. Shah, A. N. Mian, S. Mumtaz, M. Wen, T. Hong, and M. Kadoch, "Protocol stack perspective for low latency and massive connectivity in future cellular networks," in *Proc. IEEE Int. Conf. Commun. (ICC)*, Shanghai, China, 2019, pp. 1–7.

[11] M. Cheffena, "Industrial wireless communications over the millimeter wave spectrum: Opportunities and challenges," *IEEE Commun. Mag.*, vol. 54, no. 9, pp. 66–72, Sep. 2016.

[12] V. N. Swamy *et al.*, "Cooperative communication for high-reliability low-latency wireless control," in *Proc. Int. Conf. Commun. (ICC)*, London, U.K., 2015, pp. 4380–4386.

[13] S. W. H. Shah, A. N. Mian, S. Mumtaz, and J. Crowcroft, "System capacity analysis for ultra-dense multi-tier future cellular networks," *IEEE Access*, vol. 7, pp. 50503–50512, 2019.

[14] M. Haenggi, *Stochastic Geometry for Wireless Networks*, Cambridge, U.K.: Cambridge Univ. Press, 2012.

[15] S. A. Ayoughi, W. Yu, S. R. Khosravirad, and H. Viswanathan, "Interference mitigation for ultrareliable low-latency wireless communication," *IEEE J. Sel. Areas Commun.*, vol. 37, no. 4, pp. 869–880, Apr. 2019.

[16] G. Ghatak, "Cooperative relaying for URLLC in V2X networks," *IEEE Wireless Commun. Lett.*, vol. 10, no. 1, pp. 97–101, Jan. 2021.

[17] X. Li, D. Li, J. Wan, C. Liu, and M. Imran, "Adaptive transmission optimization in SDN-based industrial Internet of Things with edge computing," *IEEE Internet Things J.*, vol. 5, no. 3, pp. 1351–1360, Jun. 2018.

[18] R. Jurdi, S. R. Khosravirad, and H. Viswanathan, "Variable-rate ultra-reliable and low-latency communication for industrial automation," in *Proc. 52nd Annu. Conf. Inf. Sci. Syst. (CISS)*, Princeton, NJ, USA, 2018, pp. 1–6.

[19] N. Brahmi, O. N. C. Yilmaz, K. W. Helmersson, S. A. Ashraf, and J. Torsner, "Deployment strategies for ultra-reliable and low-latency communication in factory automation," in *Proc. IEEE Globecom Workshops (GC Wkshps)*, San Diego, CA, USA, Dec. 2015, pp. 1–6.

[20] J. Park and M. Bennis, "URLLC-eMBB slicing to support VR multimodal perceptions over wireless cellular systems," in *Proc. IEEE Global Commun. Conf. (GLOBECOM)*, Abu Dhabi, UAE, 2018, pp. 1–7.

[21] Y. Liu, Y. Deng, M. Elkashlan, A. Nallanathan, and G. K. Karagianni, "Analyzing grant-free access for URLLC service," *IEEE J. Sel. Areas Commun.*, vol. 39, no. 3, pp. 741–755, Mar. 2021.

[22] R. Candell *et al.*, "Industrial wireless systems: Radio propagation measurements," Nat. Inst. Stand. Technol., Gaithersburg, MD, USA, Rep. 1951, Jan. 2017. [Online]. Available: doi.org/10.6028/NIST.TN.1951

[23] T. S. Rappaport, "Indoor radio communications for factories of the future," *IEEE Commun. Mag.*, vol. 27, no. 5, pp. 15–24, May 1989.

[24] B. Matérn, "Spatial variation: Meddelanden från statens skogsforskningsinstitut," *Lecture Notes in Statistics*, vol. 36. New York, NY, USA: Springer, 1960, p. 21.

[25] V. N. Swamy *et al.*, "Real-time cooperative communication for automation over wireless," *IEEE Trans. Wireless Commun.*, vol. 16, no. 11, pp. 7168–7183, Nov. 2017.

Authorized licensed use limited to: CEA GRENOBLE. Downloaded on October 13,2022 at 10:28:49 UTC from IEEE Xplore. Restrictions apply.

[26] H. Viswanathan and P. E. Mogensen, "Communications in the 6G era," *IEEE Access*, vol. 8, pp. 57063–57074, 2020.

[27] *NOKIA*. Accessed: Aug. 3, 2021. [Online]. Available: https://www.nokia.com/about-us/news/releases/2019/09/10/nokia-ntt-docomo-and-omron-bring-5g-to-the-factory-floor-in-industry-40-trial/

[28] Z. Khalid and S. Durrani, "Distance distributions in regular polygons," *IEEE Trans. Veh. Technol.*, vol. 62, no. 5, pp. 2363–2368, Jun. 2013.

[29] S. N. Chiu *et al.*, *Stochastic Geometry and its Applications*. Chichester, U.K.: Wiley, 2013.

[30] K. Yu, Y. Wang, J. Yu, D. Yu, X. Cheng, and Z. Shan, "Localized and distributed link scheduling algorithms in IoT under Rayleigh fading," *Comput. Netw.*, vol. 151, pp. 232–244, Mar. 2019.

[31] A. Pandey, P. Tiwary, S. Kumar, and S. K. Das, "Adaptive mini-batch gradient-ascent-based localization for indoor IoT networks under Rayleigh fading conditions," *IEEE Internet Things J.*, vol. 8, no. 13, pp. 10665–10677, Jul. 2021.

[32] J. Zong *et al.*, "Smart user pairing for massive MIMO enabled industrial IoT communications," in *Proc. IEEE INFOCOM Conf. Comput. Commun. Workshops (INFOCOM WKSHPS)*, Toronto, ON, Canada, 2020, pp. 207–212.

[33] M. Haenggi, J. G. Andrews, F. Baccelli, O. Dousse, and M. Franceschetti, "Stochastic geometry and random graphs for the analysis and design of wireless networks," *IEEE J. Sel. Areas Commun*, vol. 27, no. 7, pp. 1029–1046, Sep. 2009.

Gourab Ghatak (Member, IEEE) received the B.Tech. degree from the National Institute of Technology Durgapur, Durgapur, India, in 2013, the M.Tech. degree from the Indian Institute of Technology Kanpur, Kanpur, India, in 2015, and the Ph.D. degree with a thesis on multi-RAT 5G networks from CEA-LETI, Grenoble, France, and Telecom ParisTech (ENST), Paris, France, in 2019.

He is an Assistant Professor with the Indraprastha Institute of Information Technology Delhi, New Delhi, India. During his master's, he was a DAAD Research Scholar with the Vodafone Chair Mobile Communications Systems, Technische Universitat Dresden, Dresden, Germany, from 2014 to 2015, where he worked on channel estimation schemes for GFDM. He is the main inventor of four patents and the author of several journals and conference publications.

Dr. Ghatak has won the Best Paper Award in the 4th International Workshop on Smart Wireless Communications, Rome, Italy, in 2017.

Saeed R. Khosravirad (Member, IEEE) received the B.Sc. degree from the Department of Electrical and Computer Engineering, University of Tehran, Tehran, Iran, the M.Sc. degree from the Department of Electrical Engineering, Sharif University of Technology, Tehran, and the Ph.D. degree in telecommunications from McGill University, Montreal, QC, Canada, in 2015.

From 2018 to 2019, he was with the Electrical and Computer Engineering Department, University of Toronto, Toronto, ON, Canada, as a Visiting Scholar. He is a Member of Technical Staff with Nokia Bell Labs, Murray Hill, NJ, USA, where he is currently leading research projects, investigating various aspects of radio access for industrial IoT. In this role, he contributes to innovating the future generation of wireless networks with ultra reliable and low latency communications technology to enable the wireless industrial revolution. His research fields of interest include wireless communications theory, cellular network technologies with emphasis on ultrareliable communication for industrial automation, and radio resource management for 5G and beyond.

Dr. Khosravirad is an Editor of the IEEE TRANSACTIONS ON WIRELESS COMMUNICATIONS and an Guest Editor of the *IEEE Wireless Communications Magazine*.

Antonio De Domenico received the M.Sc. degree in telecommunication engineering from the University of Rome "La Sapienza," Rome, Italy, in 2008, and the Ph.D. degree in telecommunication engineering from the University of Grenoble, Grenoble, France, in 2012.

From 2012 to 2019, he was a Research Engineer with CEA LETI-MINATEC, Grenoble. In 2018, he was a Visiting Researcher with the University of Toronto, Toronto, ON, Canada. Since 2020, he has been a Senior Researcher with Huawei Technologies, Paris Research Center, Paris, France. He is the main inventor or a co-inventor of 18 patents. His research interests include cloud-enabled heterogeneous wireless networks, millimeter-wave-based communications, machine learning, and green communications.

Dr. De Domenico is currently an Editor of *Wireless Communications and Mobile Computing*.

Authorized licensed use limited to: CEA GRENOBLE. Downloaded on October 13,2022 at 10:28:49 UTC from IEEE Xplore. Restrictions apply.